

X-ray-absorption study of rhenium L_3 and L_1 edges in ReO_3 : Multiple-scattering approach

A. Kuzmin and J. Purans

Institute of Solid State Physics, University of Latvia, Kengaraga 8, 226063 Riga, Latvia

M. Benfatto and C. R. Natoli

*Laboratori Nazionali di Frascati dell'Istituto Nazionale di Fisica Nucleare,
Casella Postale 13, I-00044 Frascati, Italy*

(Received 20 July 1992)

We present *ab initio* calculations of x-ray-absorption fine structure for the Re L_3 and L_1 edges in crystalline ReO_3 based on an exact curved-wave multiple-scattering approach. Good agreement between theoretical and experimental data has been found for both edges. We show that (1) as expected, the contribution of multiple-scattering signals from linear chains, like Re-O-Re and O-Re-O, is very large both in the L_3 - and L_1 -edge spectra due to the strong focusing effect caused by the middle atom; (2) the additional difference between two edges, besides the one in central-atom phase shifts and the π factor, originates from the geometrical dependence of multiple-scattering terms on the final l state, especially for paths forming a right angle at the absorbing atom; (3) the fine structure above the L_1 edge is a superposition of two signals from L_1 and L_2 edges with a very significant contribution of the latter.

I. INTRODUCTION

In this paper we present an *ab initio* curved-wave multiple-scattering analysis of x-ray-absorption fine structure (XAFS) of the Re L_3 and L_1 edges in ReO_3 .

Rhenium oxide has at atmospheric pressure a nondistorted perovskite lattice, which consists of regular ReO_6 octahedra with the rhenium atoms at the center.¹ These octahedra are connected by apexes with the bonding angle equal to 180° . Thus the large gap between the first (Re-O, $R=1.875 \text{ \AA}$) and second (Re-Re, $R=3.75 \text{ \AA}$) coordination shells allows the observation of well-isolated peaks coming from multiple-scattering processes occurring mainly in the first (oxygen) coordination shell, which are present in the Fourier transform (FT) of an XAFS signal with a good signal-to-noise ratio. Moreover, the presence of linear chains (Re-O-Re) leads to a strong focusing effect, which results in the significant increase of the Fourier-transform amplitude of the signal from the second coordination shell. This peculiarity was experimentally observed in the Re L_3 -edge XAFS by Aldberding *et al.*² Several attempts²⁻⁴ using different approaches have been made earlier to explain qualitatively this fact. The most successful results have been obtained by Vedrinskii, Bugaev, and Levin.³ They found that the main contribution into the near-edge XAFS is given by signals from nearly linear atomic chains originating and terminating at the absorbing rhenium atom, but a detailed interpretation of the origin of the various features in the Fourier transform was not given. Moreover, all previous works have been based on data from Ref. 2 done on an experimental setup for pressure-dependent measurements that naturally led to an increase of noise.

In previous papers⁵ two of us presented low-noise experimental data for the Re L_3 and L_1 edges. The analysis of the first coordination shell, done in the single-

scattering plane-wave approximation with amplitudes and phases calculated by McKale *et al.*,⁶ showed good agreement with x-ray-diffraction data. In the last work,⁷ we applied the *fast spherical approximation* to the multiple-scattering study of several compounds including ReO_3 . The detailed analysis of the Re L_3 -edge XAFS has shown that in order to simulate the experimental spectrum it is enough to take into account single-scattering contributions within the first five coordination shells and a number of multiple-scattering paths within the first and second shells. It was found that multiple-scattering paths with the angle at the central absorbing atom equal to 90° , which contribute to the L_3 edge, vanish in the case of K and L_1 edges as a result of the Legendre polynomial term [see Eqs. 6(a) and 6(b) in Ref. 7].

In this work the precise analysis of XAFS from two edges (L_3 and L_1) using the exact multiple-scattering formalism⁸ is considered. In Sec. II we describe experimental details and a step-by-step procedure of the x-ray-absorption spectra treatment. Section III is devoted to methods of computation. Section IV contains results of theoretical calculations and the comparative analysis with experiments both for L_3 and L_1 edges, and Sec. V contains a summary and the main conclusions.

II. EXPERIMENTAL AND DATA ANALYSIS

X-ray-absorption spectra of the Re L_3 and L_1 edges in ReO_3 (Fig. 1) were recorded in transmission mode at room temperature at the ADONE storage ring (Laboratori Nazionali di Frascati) on the BX-1 PWA beam line using synchrotron radiation from a wiggler source.⁵ The storage ring ADONE operated at 20–50 mA and 1.5 GeV with a wiggler current of 4000 A. Data were collected using the standard scheme with two ion chambers filled with krypton gas. The Si(111) and Si(220) channel-

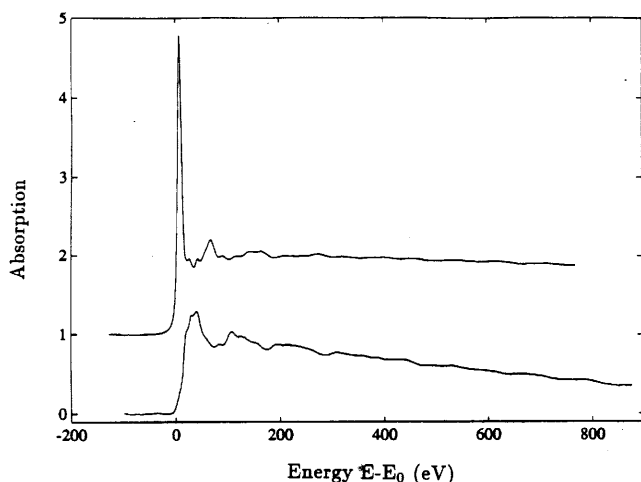


FIG. 1. Experimental x-ray-absorption spectra of the Re L_3 (upper curve) and L_1 edges in ReO_3 . The energy origin is chosen at the absorption edge.

cut crystal monochromators were used for L_3 and L_1 edges, and the energy resolution was estimated to be equal to about 1 eV. The sample was prepared from polycrystalline ReO_3 , which was finely ground and deposited on an organic filter.

The data analysis was carried out following the standard procedure.⁹ The background contribution from previous edges, $\mu_b(E)$, was approximated according to the Victoreen rule ($\mu_b = A/E^3 + B/E^4$) and subtracted from the experimental spectrum $\mu(E)$. Then the atomiclike term $\mu_0(E)$ was found by a cubic-spline approximation, and the XAFS signal $\chi(k)$ was determined as $\chi(k) = (\mu - \mu_b - \mu_0) / \mu_0$, where the photoelectron wave vector k is defined as $k = [(2m/\hbar^2)E]^{1/2}$, where E is the photoelectron kinetic energy measured from the inner-core photoemission threshold (vacuum level). Based on Ref. 10, we locate it some 5 eV above the white line. We have referred the k scale of the calculated spectra to the same origin. The reason for doing this comes from the fact that this is the only physical parameter on which to align measured and calculated spectra, all the more that we use an energy-dependent exchange and correlation potential of the Hedin-Lundqvist type (see below), therefore without a fixed *muffin-tin* reference level. The vacuum level can either be measured or estimated on the basis of theoretical calculations.¹¹ In any case there is no adjustment between calculated and experimental spectra so that the absolute phase agreement between them is an *ab initio* one. Note that all Fourier transforms reported in this paper have been done without phase correction, which means that the positions of the peaks are shifted from their true crystallographic values.

III. METHOD OF CALCULATION

In multiple-scattering theory, the oscillatory structure χ^l past the absorption edge of orbital type l can be described by a scattering series⁸

$$\chi^l = \sum_{n=2}^{\infty} \chi_n^l, \quad (1)$$

where χ_n^l represents contributions from all processes, where the excited photoelectron experiences $(n-1)$ scatterings by the surrounding atoms before returning to the photoabsorber. Because of the path lengths, the finite lifetime of the excitation, and cancellation effects, usually only a few terms of this series produce a significant contribution to the total signal especially at high energies. The first three of them correspond to processes of single (χ_2^l), double (χ_3^l), and triple (χ_4^l) scatterings, and the exact analytical expressions were found for them earlier in the curved-wave formalism.^{8,12} In this work the MSXAS code¹³ was used for their computation.

A ten-shell cluster around the absorbing Re_0 atom, consisting of 189 atoms inside the sphere with 8.5 Å radius, was used in potential and partial phase-shift calculations. The cluster dimensions were estimated from a mean-free-path calculation (see below) and were taken in such way to have a good approximation of the potential for all those atoms, whose scattering signals produce a significant contribution to the XAFS spectrum. Thus each such atom was surrounded by at least two shells. The total cluster potential was constructed from a set of

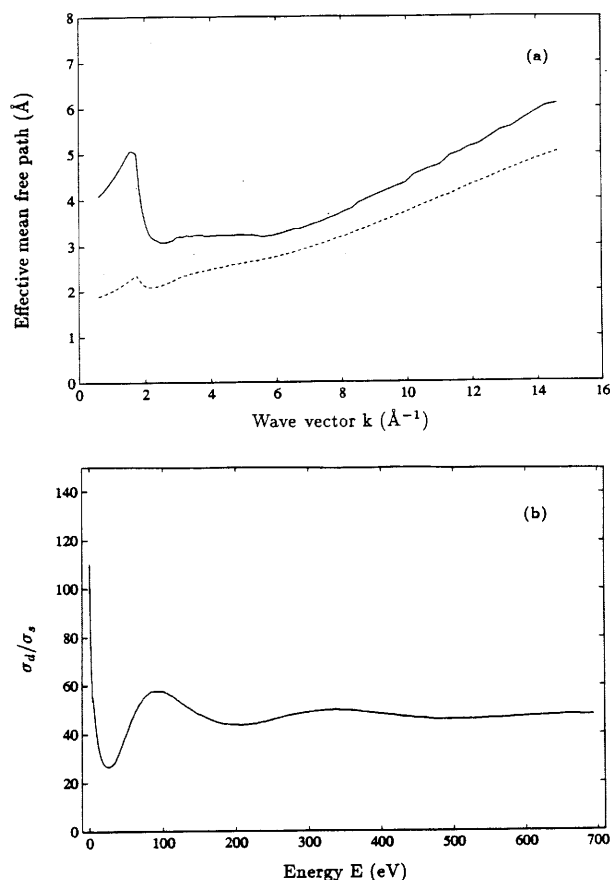


FIG. 2. (a) Effective mean free paths $\lambda(k)$ calculated from the imaginary part of the complex Hedin-Lundqvist potential for the Re L_3 (solid line) and L_1 (dashed line) edges. (b) Ratio $\sigma_d(E)/\sigma_s(E)$ of absorption cross sections for d (σ_d) and s (σ_s) final states in the case of the Re L_3 edge.

muffin-tin (MT) atomic potentials as described in Ref. 8. The MT radii were equal to 1.0647 Å for rhenium and 0.9978 Å for oxygen. For the absorbing (rhenium) atom, its final-state density was taken to be fully relaxed with a core hole localized in the appropriate shell.

The complex Hedin-Lundqvist (HL) potential was used to approximate the exchange-correlation term. Thus the correction to the XAFS amplitude caused by the inelastic losses of the photoelectron in extrinsic channels through plasmon excitations has been automatically included. The amplitude damping due to the core-hole finite lifetime was taken into account through the empirically determined core-level widths $\Gamma_{L_3} = 3.4$ eV and $\Gamma_{L_1} = 5.9$ eV.¹⁴ The effective mean free paths $\lambda(k)$ for both edges calculated from the imaginary part of the HL potential including the core-hole width are shown in Fig. 2(a). One can see that only atoms located inside a sphere of 6 Å radius can make a significant contribution into the XAFS spectrum. This figure coincides with the position of well-resolved peaks in the Fourier transforms of experimental spectra [see Figs. 3(b) and 8(b)].

Let us note that in the calculation of the L_3 -edge XAFS only transitions to the final states with d symmetry have been considered, neglecting the contribution from s final states. In fact, the calculated ratio $\sigma_d(E)/\sigma_s(E)$ of absorption cross sections, corresponding to the transition into d (σ_d) and s (σ_s) final states, is equal to ≈ 50 in the case of the Re L_3 edge [Fig. 2(b)].

IV. RESULTS AND DISCUSSION

A set of atomic coordinates, used in the calculation of the separate scattering paths, is shown in Table I. The high symmetry of the cluster allows us to take into account only ten atoms inside the first five coordination shells to describe multiple-scattering paths which produce the main contributions to XAFS (see Table II). In the calculated spectra, all parameters except the Debye-Waller (DW) factors were taken in an *ab initio* way. The values of the DW factors were taken into account through the $\exp(-2\sigma^2k^2)$ terms and were found by a fitting procedure separately for each multiple-scattering path. We realize that such an approach does not ade-

TABLE I. Coordinates of atoms used in calculations of scattering paths. Re_0 corresponds to the central absorbing atom ($a = 3.750$ Å is the lattice parameter).

Atom	Shell number	X (Å)	Y (Å)	Z (Å)
Re_0	0	0	0	0
O_1	1	$-\frac{1}{2}a$	0	0
O_2	1	0	$\frac{1}{2}a$	0
O_3	1	0	0	$\frac{1}{2}a$
O_4	1	$\frac{1}{2}a$	0	0
Re_5	2	a	0	0
O_6	3	a	$\frac{1}{2}a$	0
Re_7	4	a	a	0
O_8	5	$\frac{3}{2}a$	0	0
O_9	5	a	a	$\frac{1}{2}a$

TABLE II. Scattering paths used in calculation of the Re L_3 - and L_1 -edge XAFS. The numbers in paths correspond to atoms in Table I.

Type	Name	Path	Degeneracy	
Single scattering	XSS1	0-1-0	6	
	XSS2	0-5-0	6	
	χ_2	XSS3	0-6-0	24
		XSS4	0-7-0	12
	Double scattering	XSS5	0-8-0	24
		XSS6	0-9-0	6
XDS1		0-1-2-0	24	
χ_3	XDS2	0-1-4-0	6	
	XDS3	0-4-5-0	12	
	XDS4	0-4-6-0	48	
	Triple scattering	XTS1	0-1-0-1-0	6
XTS2		0-1-0-2-0	24	
χ_4		XTS3	0-1-2-1-0	24
		XTS4	0-1-2-4-0	24
XTS5		0-1-2-3-0	48	
XTS6		0-2-1-4-0	24	
XTS7		0-4-6-4-0	24	
XTS8		0-1-0-4-0	6	
XTS9		0-4-5-4-0	6	

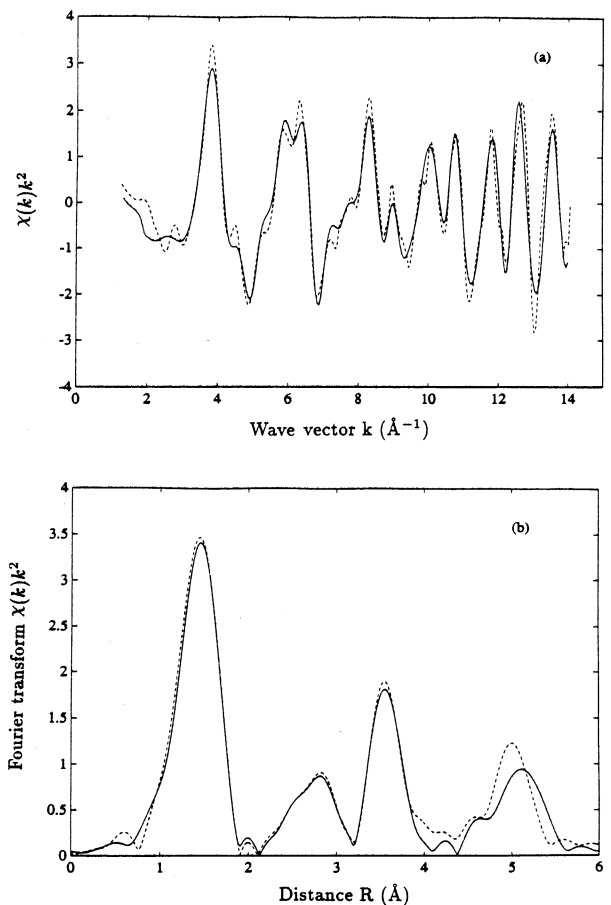


FIG. 3. (a) Experimental (dashed line) and calculated (solid line) XAFS spectra $\chi(k)k^2$ of the Re L_3 edge. (b) Fourier transforms of spectra shown in (a).

quately describe the effect of thermal vibrations, and we consider it as a first approximation. In the future a more precise analysis will be done using the existing theory.¹⁵

In Fig. 3 experimental and calculated XAFS spectra $\chi(k)k^2$ for the Re L_3 edge and their Fourier transforms are presented. The agreement obtained is very good in

spite of the large number of multiple-scattering contributions whose separate signals are shown in Fig. 4. As was mentioned previously,⁷ the rhenium and oxygen atoms contribute at different energy ranges because of the peculiarities of their scattering amplitudes. Note that the increase of the signal $\chi(k)k^2$ from rhenium atoms at high

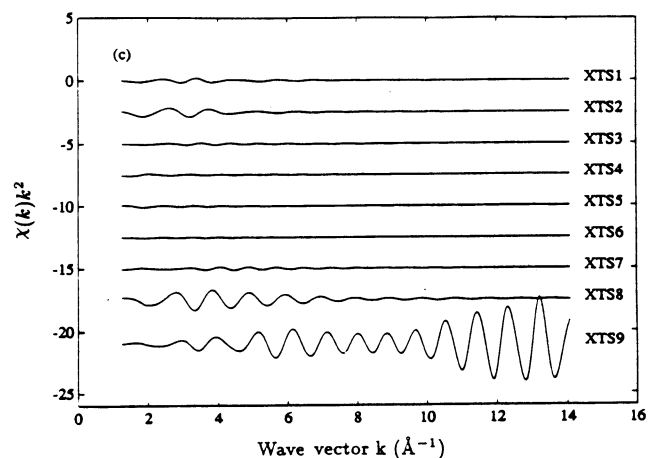
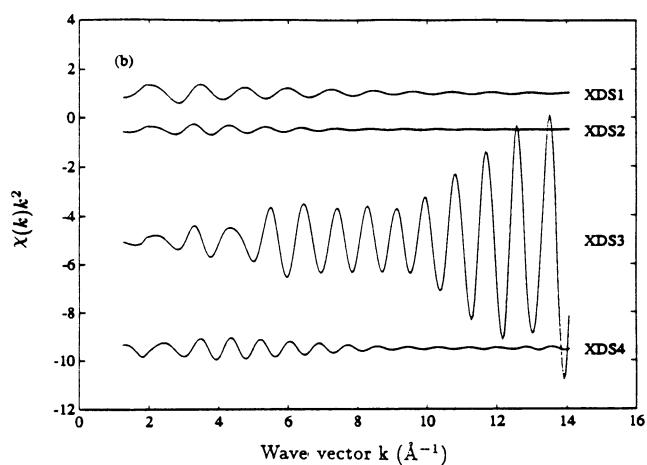
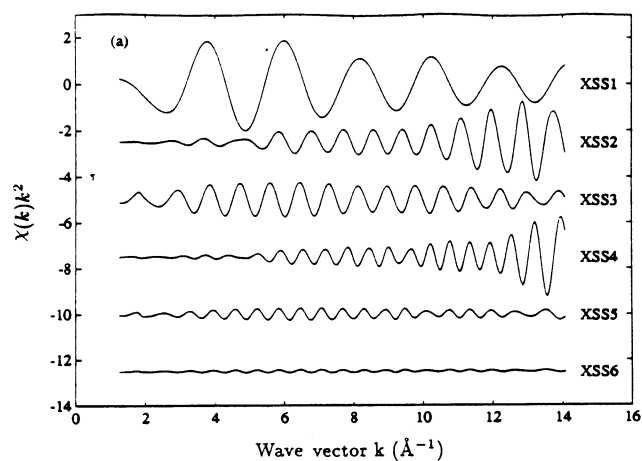


FIG. 4. Separating multiple-scattering contributions to the L_3 XAFS: (a) single scattering, (b) double scattering, and (c) triple scattering. For an explanation of path's names, see Table II.

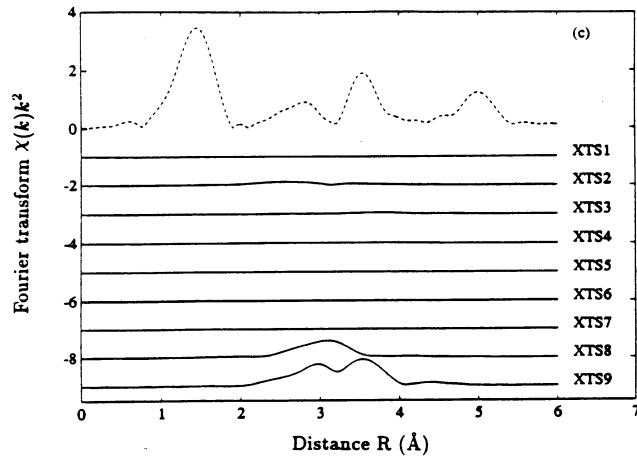
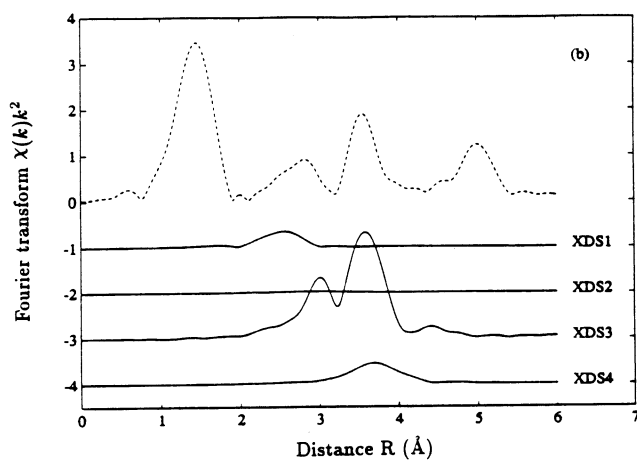
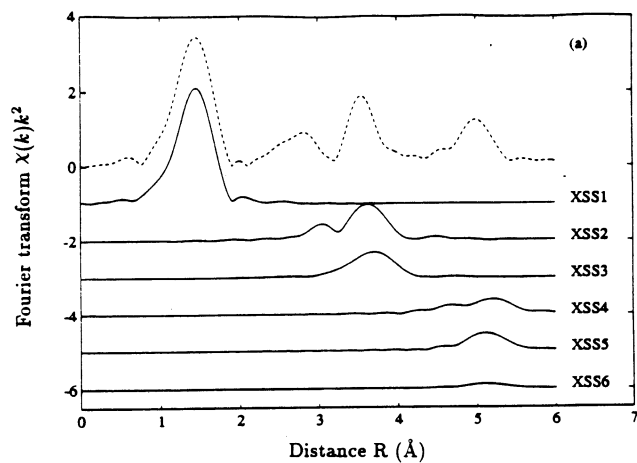


FIG. 5. Fourier transforms (FT's) of multiple-scattering signals shown in Fig. 4. The dashed line represents FT's of the experimental signal.

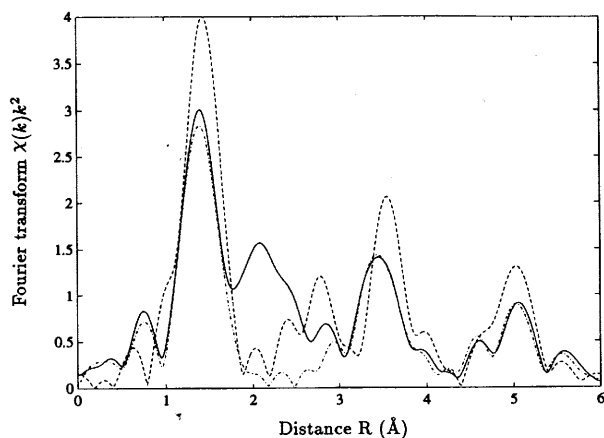


FIG. 6. Fourier transforms (FT's) of the experimental L_3 (dashed line) and L_1 (solid line) XAFS spectra. The FT's of the L_1 XAFS spectrum after subtraction of contribution from the L_2 edge is shown by the dot-dashed line.

energies implies the need to measure a long low-noise spectrum for its quantitative analysis.

Figure 5, where the Fourier transforms of the experimental spectrum and separate multiple-scattering signals are shown, gives us clear interpretation⁷ of the origin of all peaks. The main peak at ≈ 1.4 Å corresponds to the six oxygen atoms in the first coordination shell. The second one, located in the range from 2.2 to 4.2 Å with a double-hump shape, has a complicated nature. Its left-side maximum is mainly due to the multiple-scattering signals in the first oxygen shell (XDS1 and XTS8), while the right-side maximum owes its intensity to various multiple-scattering contributions: the strongest one due to a focusing effect in the chain $\text{Re}_0\text{-O-Re}$ (XDS3), the double-scattering contributions from oxygen atoms in the first and third shells (XDS4) and single-scattering contributions from rhenium (XSS2) and oxygen (XSS3) atoms located in the second and third shells. It must be noted

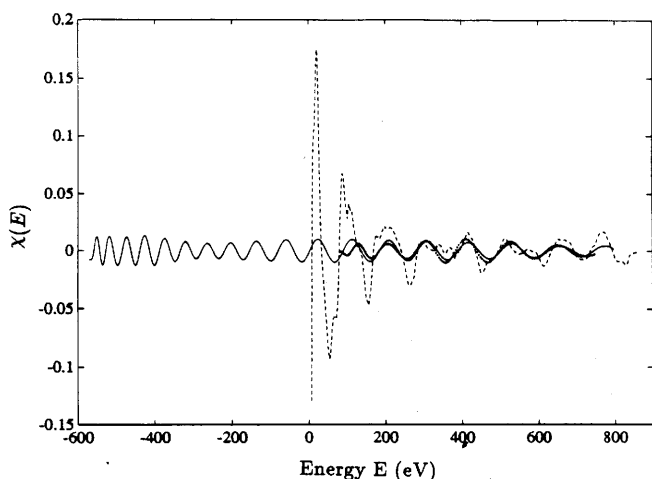


FIG. 7. Experimental L_1 -edge XAFS $\chi(E)$ (dashed line). The dotted line is its back Fourier transform in the range 1.8–2.6 Å. The solid line shows a calculated multiple-scattering signal for the L_2 edge from the Re-O-Re chain.

that the double-hump shape of the backscattering amplitude of rhenium (see signals XSS2, XDS3, and XTS9 in Fig. 5), which is typical for all heavy atoms, leads to considerable overlap of the left- and right-side maxima and does not allow a separation of the above-mentioned contributions. The last peak at ≈ 5 Å is a superposition of single-scattering signals from rhenium (XSS4) and oxygen (XSS5 and XSS6) atoms in the fourth and fifth shells. Thus the XAFS from the L_3 edge can be well and easily interpreted. Note that a large number of oxygens located in the third [$R(\text{Re-O}) \approx 4.19$ Å] and fifth [$R(\text{Re-O}) = 5.625$ Å] shells gives a significant contribution to the total signal in spite of the large distances and high amplitude of their thermal vibrations. Among multiple-scattering paths, the signals from linear chains both in the first (O- Re_0 -O) and second (Re_0 -O-Re) shells have the largest amplitude and are the most important. This is due to the focusing role of the middle atom (Re or O) whose high forward-scattering amplitude increases essentially the final signal. Moreover, the path (XDS1) with the angle at the central atom equal to 90° gives a non-negligible contribution in the case of the L_3 edge too.

The difference between L_3 and L_1 edges reflects the different orbital symmetry of the final states, which implies a different central-atom phase shift and the factor $(-1)^l$ (π factor) which stands in front of any signal $\chi_n^l(k)$.^{8,16} However, these factors do not influence the

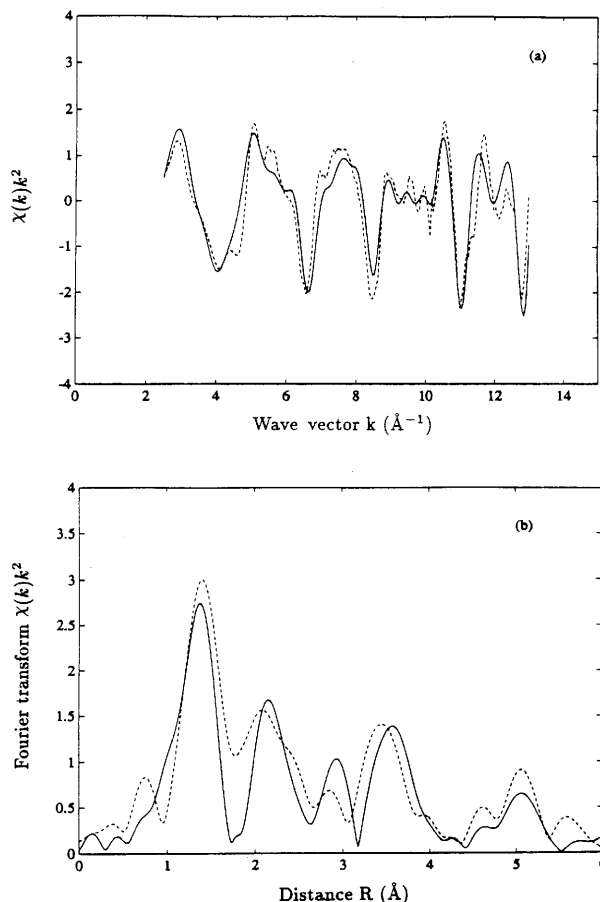


FIG. 8. (a) Experimental (dashed line) and calculated (solid line) XAFS spectra $\chi(k)k^2$ of the Re L_1 edge. (b) Fourier transforms of spectra shown in (a).

modulus of the Fourier transform. By looking at the dashed and solid curves in Fig. 6, which correspond to the Fourier transforms of the L_3 and L_1 experimental signals, we observe three main differences: (1) The magnitude of the L_3 edge signal is higher, (2) the positions of peaks do not coincide, and (3) a large additional signal in the range 1.8–2.6 Å appears in the case of the L_1 edge.

As we found, the first two differences are accounted for by the core-hole widths and phase shifts caused by the absorbing rhenium atom. To explain the third, we observe that the energy separation between the L_2 and L_1 edges of rhenium is sufficiently small, ≈ 568 eV. So the idea is that the origin of the additional contribution comes from the L_2 XAFS signal which extends into the

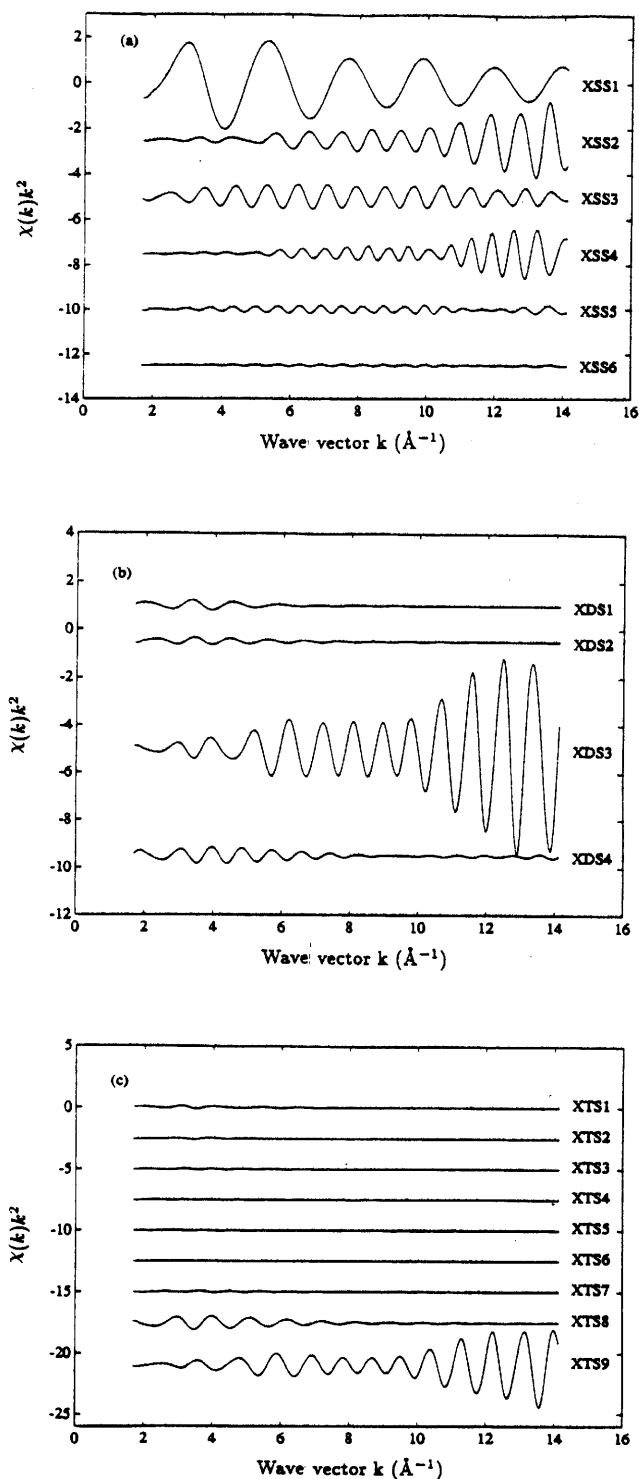


FIG. 9. Separating multiple-scattering contributions to the L_1 XAFS: (a) single scattering, (b) double scattering, and (c) triple scattering. For an explanation of path's names, see Table II.

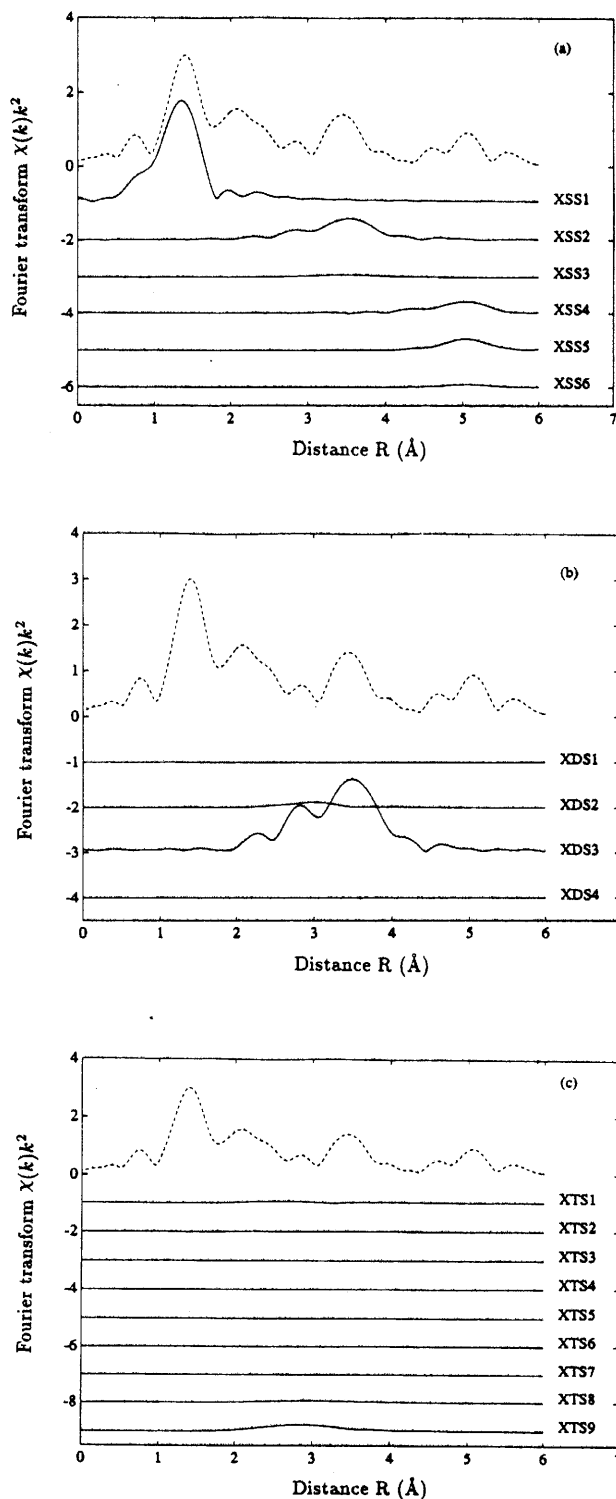


FIG. 10. Fourier transforms (FT's) of multiple-scattering signals shown in Fig. 9. The dashed line represents FT's of the experimental signal.

region above the L_1 edge. Such an effect was observed earlier for L edges of gold.¹⁷ In Fig. 7 the experimental L_1 -edge XAFS $\chi(E)$ (dashed line) and its back Fourier transform in the range 1.8–2.6 Å (dotted line) are shown together with the calculated multiple-scattering signal of the L_2 edge generated in the Re-O-Re chain (solid line). The good agreement between the last two signals allows us to conclude that the fine structure past the Re L_1 edge in ReO_3 has a composite nature belonging both to the L_1 and L_2 XAFS with a very significant contribution from the last one as a result of the presence of the strong focusing effect.

The calculation of the L_1 XAFS has been made using the same set of multiple-scattering paths as for the L_3 edge (see Table II) plus the focusing contribution from the L_2 edge. The experimental and total calculated signals $\chi(k)k^2$ and their Fourier transforms are shown in Fig. 8. The agreement here is not so good as for the L_3 edge because of incomplete treatment of the contaminating signal coming from the L_2 edge, which might contain additional contributions not taken into account. The separate multiple-scattering contributions to the L_1 XAFS and their Fourier transforms are presented in Figs. 9 and 10. The origin of all peaks can be explained in the same way as for the L_3 edge except those in the range 2–3 Å, which correspond to multiple scatterings in the first coordination shell. In fact, the comparison of the Fourier transforms for the L_3 and L_1 (after subtraction of the contribution from the L_2 edge) experimental signals (Fig. 6) shows a big difference in the interval from 2 to 3 Å. In this region, in the case of the L_1 edge, one can see the absence of some signal. From the analysis of the L_3 edge, it is known that the multiple-scattering path (XDS1) with the angle at the central absorbing atom equal to 90° is mainly responsible for the left side of the peak at ≈ 2.5 Å. If we look at Figs. 9(b) and 10(b), then

it is clear that in the case of the L_1 edge the contribution of the same path is negligibly small. This is a consequence of the fact that in the fast spherical approximation such paths are proportional to $P_l(\cos 90^\circ)$ so that they produce zero contribution for K and L_1 ($l=1$) edges (see Sec. I and Ref. 7). Thus the difference between L_1 and L_3 edges, apart from reflecting the difference in central-atom phase shifts, the π factor, and core-hole-level widths, originates also from the geometrical dependence of multiple-scattering terms on the final l states. This latter cannot be compensated by the procedure suggested in Ref. 16.

V. SUMMARY AND CONCLUSIONS

We have presented an *ab initio* analysis of x-ray-absorption fine structure for the Re L_3 and L_1 absorption edges in crystalline ReO_3 based on the exact curved-wave multiple-scattering approach.

We have found that multiple-scattering contributions in the first and second coordination shells are very important for interpretation of XAFS for both edges. Moreover, their presence makes it impossible to generate the L_1 XAFS from the L_3 XAFS and vice versa, as was suggested previously.¹⁶ We have also shown that the fine structure above the L_1 edge is a superposition of two signals from L_1 and L_2 edges, this latter contribution being due mainly to multiple scatterings in the linear Re-O-Re chain.

ACKNOWLEDGMENTS

A.K. and J.P. wish to thank the Laboratori Nazionali di Frascati for hospitality and support during their stay there. They are also thankful to Professor E. Burattini and his collaborators for the possibility to carry out the experiments at the "PWA" EXAFS station.

¹J. E. Jørgensen, J. D. Jørgensen, B. Batlogg, J. P. Remeika, and J. D. Axe, *Phys. Rev. B* **33**, 4793 (1986).
²N. Alberding, E. D. Crozier, R. Ingals, and B. Houser, *J. Phys. (Paris)* **47**, 681 (1986).
³R. V. Vedrinskii, L. A. Bugaev, and I. G. Levin, *Phys. Status Solidi B* **150**, 307 (1988).
⁴V. Frizsche, *J. Phys. Condens. Matter* **1**, 7715 (1989).
⁵A. Balerna, E. Bernieri, E. Burattini, A. Kuzmin, A. Lusic, J. Purans, and P. Cizmach, *Nucl. Instrum. Methods A* **308**, 234 (1991); **308**, 240 (1991).
⁶A. G. McKale, B. W. Veal, A. P. Paulikas, S. K. Chan, and G. S. Knapp, *J. Am. Chem. Soc.* **110**, 3763 (1988).
⁷A. Kuzmin and J. Purans (unpublished).
⁸M. F. Ruiz-Lopez, M. Loos, J. Goulon, M. Benfatto, and C. R. Natoli, *Chem. Phys.* **121**, 419 (1988); C. Brouder, M. F. Ruiz-Lopez, R. F. Pettifer, M. Benfatto, and C. R. Natoli, *Phys. Rev. B* **39**, 1488 (1989).
⁹B. K. Teo, *EXAFS: Basic Principles and Data Analysis* (Springer-Verlag, Berlin, 1986).

¹⁰L. F. Mattheiss, *Phys. Rev.* **181**, 987 (1969).
¹¹T. A. Tyson, K. O. Hodgson, C. R. Natoli, and M. Benfatto, *Phys. Rev. B* **46**, 5997 (1992).
¹²C. R. Natoli and M. Benfatto, *J. Phys. (Paris) Colloq.* **47**, (C8)-11 (1986); S. J. Gurman, N. Binsted, and I. Ross, *J. Phys. C* **19**, 1845 (1986).
¹³M. F. Ruiz-Lopez, F. Bohr, A. Filipponi, A. Di Cicco, T. A. Tyson, M. Benfatto, and C. R. Natoli, in *X-Ray Absorption Fine Structure*, edited by S. S. Hasnain (Ellis Horwood, New York, 1991), p. 75.
¹⁴K. D. Sevier, *Low Energy Electron Spectrometry* (Wiley, New York, 1972).
¹⁵M. Benfatto, C. R. Natoli, and A. Filipponi, *Phys. Rev. B* **40**, 9626 (1989).
¹⁶J. Chaboy, J. Garcia, M. Sanchez del Rio, and A. Marcelli, in *X-Ray Absorption Fine Structure*, edited by S. S. Hasnain (Ellis Horwood, New York, 1991), p. 62.
¹⁷P. Rabe, G. Tolkiehn, and A. Werner, *J. Phys. C* **12**, 899 (1979).